From Th-Rhabdophane to Monazite-Cheralite Solid Solutions: Thermal Behavior of Nd 1–2 x Th x Ca x PO 4 × n H 2 O (x = 0–0.15)

Danwen Qin, Adel Mesbah, Nicolas Clavier, Stephanie Szenknect, Nicolas Dacheux

From Th-rhabdophane to monazite-cheralite solid solutions: thermal behavior of $Nd_{1-2x}Th_xCa_xPO_4 \cdot n\ H_2O$ (x = 0 - 0.15)

Danwen Qin[a], Adel Mesbah[a, *], Nicolas Clavier[a,*], Stéphanie Szenknect[a], Nicolas Dacheux[a]

[a] ICSM, CNRS, CEA, ENSCM, Univ Montpellier, Site de Marcoule, BP 17171, 30207 Bagnols/Cèze, France

Abstract

The synthesis and thermal behavior of $Nd_{1-2x}Th_xCa_xPO_4 \cdot n\ H_2O$ (x = 0 – 0.15) solid solutions crystallizing in the rhabdophane structure type was studied by combining the *in situ* high temperature PXRD, TGA and dilatometry techniques. The samples prepared under hydrothermal conditions (T = 110°C, t = 4 days) were found to follow the same dehydration process than the $NdPO_4 \cdot 0.667\ H_2O$ end-member. The temperature of maximum dehydration rate slightly increased from 210 ± 3 °C to 214 ± 3 °C with the Ca-Th coupled substitution rate. In parallel, the evolution of the unit cell parameters was also monitored by collecting *in situ* HT-PXRD data. The phase transition into the monazite-type structure occurred at higher temperature (from 650°C to 850°C) and was correlated to a temperature of maximum linear shrinkage rate increasing from 693 ± 1°C to 762 ± 1°C with the Ca-Th content. Therefore, the process of conversion leading the stabilization of $Nd_{1-2x}Th_xCa_xPO_4$ was successfully achieved.

1. Introduction

The management of radioactive waste coming from the reprocessing of nuclear spent fuel represents one of the major challenges in the nuclear power industry.[1] In this frame, a tremendous number of studies have been dedicated to the conditioning and storage of high level radioactive wastes (HLW). Particularly, glass, glass-ceramics and ceramics have been proposed as sustainable wasteforms [2-4]. In this frame, France, with the "Bataille" act, adopted in 1991, set out the legislative framework of the radioactive waste management, especially underground repository to host actinides and fission products by considering different solutions as cited above. In order to meet the requirements of this law, a particular attention was paid to the specific conditioning of actinides in tailored ceramic wasteforms, such as phosphate based materials including apatites ($Ca_{10}(PO_4)_6F_2$), [5-7] monazites ($LnPO_4$) and associated cheralites ($M^{II}M^{IV}(PO_4)_2$) [8-12] or thorium phosphate–diphosphate [13]. Monazite $LnPO_4$ with Ln = La to Gd and its related solid solutions, fulfill several requirements such as the capability to contain large amounts of actinides within its structure (up to 29 wt. % ThO_2 and 16 wt. % UO_2 in monazite ores) [14, 15], good sintering capabilities [16], high chemical durability [17, 18] and good resistance to radiation damage [19, 20].

The mechanism of actinides incorporation into the monazite structure depends on their oxidation state. For trivalent actinides (e.g. Pu, Am), the direct incorporation was already reported in respect of the $Ln_{1-x}An^{III}_xPO_4$ formula[21, 22]. On the contrary, a coupled substitution is always required to incorporate tetravalent actinides (An(IV) = Th, U, Np). Two substitution schemes were reported in literature: the first one consists of a simultaneous incorporation of a divalent element such as an alkaline earth metal and tetravalent actinide to form $Ln_{1-2x}An^{IV}_xM^{II}_xPO_4$ monazite-cheralite solid solution. The second one consists of the replacement of the phosphate groups by silicate entities to form $Ln_{1-x}An_x(PO_4)_{1-x}(SiO_4)_x$ monazite-huttonite solid solutions [14, 23, 24]. The first mechanism is by far the most documented [10] and the actinide-based monazite-cheralite solid-solutions were usually synthesized through solid-state reactions [23-29]. However, there is a growing interest in the preparation of monazites by wet chemistry routes in order to improve the homogeneity and sintering properties of the powders [16, 30, 31]. Consequently, we investigated the incorporation of tetravalent thorium into $PrPO_4$ through the $2\ Pr^{3+} \leftrightarrow Th^{4+} + Ca^{2+}$ cationic substitution [32]. A series of rhabdophane-type precursors with the general formulae $Pr_{1-2x}Th_xCa_xPO_4 \cdot n\ H_2O$ were firstly prepared by hydrothermal synthesis (110°C, 4 days), then associated monazite-cheralite solid solutions $Pr_{1-2x}Th_xCa_xPO_4$ were obtained after heat treatment at 1100 ºC for 6 hours. As the powder crystallizing in the rhabdophane structure type is considered as the stable hydrated form for light lanthanide phosphates (Ln = La-Gd) at low temperature [31], the protocol mentioned above might be suitable for other light lanthanide monazite-cheralites having the general formulae $Ln_{1-2x}Th_xCa_xPO_4$.

Nevertheless, the dehydration process and the steps associated to the thermal conversion of $Ln_{1-2x}Th_xCa_xPO_4.nH_2O$ compounds were never assessed while there are only few reports on the thermal behavior of rhabdophane $LnPO_4 \cdot nH_2O$. Indeed, Jonasson and Vance have investigated the transformation of rhabdophane to monazite for Ln = La – Dy using thermogravimetric analysis (TGA) and differential thermal analyses (DTA). They have reported dehydration temperatures ranging from 100 to 400°C while the temperature mentioned for the irreversible transformation into monazite was found between 500 and 900°C. Moreover, the conversion temperature increased with decreasing ionic radius [33]. A similar study has been done by Kijkowska[34] who reported a double endothermic effect below 300°C assigned to a two-step dehydration. Furthermore, the temperature of rhabdophane to monazite transformation was found to increase with the atomic number from below 750°C (La, Ce) to above 900°C (Tb, Dy).[34]

From the structural point of view, Mesbah *et al*. reported the dehydration process and related crystal structure changes from monoclinic $LnPO_4 \cdot 0.667\ H_2O$ to trigonal $LnPO_4$ with Ln = Nd, Sm, Gd, Eu and Dy [35]. The initial crystal structure (monoclinic C2, Z = 24) has six independent positions for the cations. One third of them is coordinated to 8 oxygen atoms from the phosphate groups to form an infinite chain (called ch1) while the other two thirds are coordinated by 9 oxygen atoms with the ninth represented by a water molecule to form a second different chain (Ch2) leading to a channeled structure oriented along [101] direction (Figure 1), where the water molecules fill those channels. During the dehydration of the rhabdophane samples, which involves a two-step process, the lanthanide phosphate first turns into the hemihydrate compound ($LnPO_4 \cdot 0.5\ H_2O$, monoclinic C2). Within this structure, there is one kind of chains formed by half of the lanthanide atoms in 8-fold coordinated while the others are 9-fold coordinated. This leads to the disappearance of the anhydrous chains and the reconstruction of the water network. However, all the chains are oriented along the [101] direction and water molecules also stay within the structure channels (Figure 1). The full dehydration towards anhydrous rhabdophane (trigonal, $P3_121$) takes place between 190°C and 240°C. Finally, the irreversible transformation into monazite occurs for temperatures above 500°C.

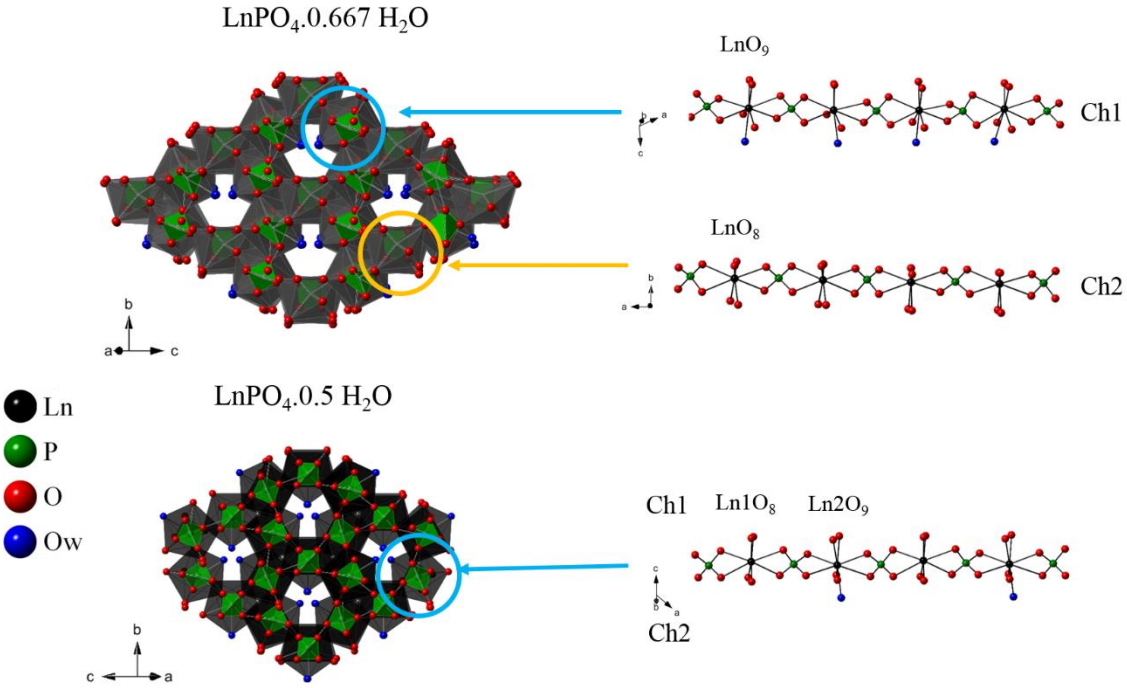

Figure 1. Representation of the chains and channels present in $LnPO_4 \cdot 0.667\ H_2O$ (top) and $LnPO_4 \cdot 0.5\ H_2O$ (bottom).[35]

In this study, single phase samples of $Nd_{1-2x}Th_xCa_xPO_4 \cdot n\ H_2O$ (x = 0 to 0.15) were prepared by wet chemistry route then their thermal conversion into the final monazite-cheralite compounds was first followed by *in situ* HT-PXRD to determine the conversion temperature range and to investigate the variation of the unit cell volume. Moreover, a coupled TGA/dilatometry study was undertaken to get better understanding of the dehydration and conversion processes.

2. Experimental

2.1. Synthesis

Following the synthesis procedure described in our previous work [32], the metal nitrate salts used (Sigma-Aldrich) were of analytical grade: $NdCl_3 \cdot 6\ H_2O$, $CaCl_2 \cdot n\ H_2O$, $Th(NO_3)_4 \cdot 4\text{-}5\ H_2O$; while acid solutions were diluted from concentrated H_3PO_4 (85% Sigma-Aldrich), HCl (37% Carlo-Erba), and HNO_3 (69.5% Carlo-Erba). In order to avoid any problem of stoichiometry due to the hygroscopic character of the salts and thus to prevent potential lack of accuracy in weighing the amount of reactants, $NdCl_3$ and $CaCl_2$ were dissolved in 0.1M HCl and $Th(NO_3)_4 \cdot 4\text{-}5\ H_2O$ in 4M HNO_3. The final concentrations were typically ranging from 0.5 to 1.5 M. They were further determined by ICP-AES. As already described, the synthesis proceeded through mixing stoichiometric amounts of neodymium and thorium into a 30 mL Teflon® container, with ten times the stoichiometric amount of calcium compared to thorium. Afterwards, 5M H_3PO_4 was added dropwise with a 3 mol.% excess with regards to Nd and Th amounts. The mixture was stirred for 15 minutes then the Teflon® container was

sealed and placed in an oven at 110°C for 4 days. The obtained precipitate was washed (twice with water and once with ethanol) by going through three centrifugation cycles (at 14500 rpm for 5 minutes). Finally, the product was dried in an oven at 90°C overnight.

2.2. Powder X-Ray Diffraction (PXRD) & *in situ* High Temperature-PXRD (HT-PXRD)

PXRD analyses were realized on a Bruker D8 advance diffractometer, equipped with Cu Kα radiation (λ = 1.54184 Å). Data collection was performed using reflection geometry with 2θ ranging from 5 to 100° with steps of Δθ = 0.019° and a step time of t = 3.68 s. In addition, a PXRD pattern of pure silicon was collected in similar conditions to be used as an external standard to extract the instrumental function. The collected powder patterns were refined by the Rietveld method with the use of the Fullprof_Suite package [36].

Moreover, in order to identify the successive dehydration steps and phase transformation, *in situ* HT-PXRD experiments were performed on the same instrument for temperatures ranging from room temperature (RT) to 1100°C with a rate of 5°C.min^{-1}. During each experiment, the PXRD patterns were collected on a set of 30 temperature set points. For each measurement, the system was held at the target temperature for 15 minutes prior the beginning of the scan from 5 to 100° (2θ, angular step of 0.014° and time step of 1.10 s). Table S1 gathers the crystal data and the refinement parameters for the $Nd_{1-2x}Th_xCa_xPO_4 \cdot n\ H_2O$ series (x = 0, 0.05 and 0.1) at 30°C, 100°C, 300°C (rhabdophane) and at 30°C (monazite-cheralite) after thermal treatment at 1100°C.

2.3. Thermo-Gravimetric Analyses (TGA) and dilatometric study

TG analyses were undertaken thanks to a Setaram Setsys Evolution apparatus equipped with a type-S thermocouple (Pt/Pt-10%Rh). After the blank was recorded using an empty alumina crucible (30 µL), about 15 mg of powder were heated in air with a rate of 5°C.min^{-1} from RT to 1000°C in order to follow the dehydration steps then the transition from rhabdophane to monazite.

Accordingly, the dilatometric measurements were conducted with a similar apparatus with thermo-mechanical analysis (TMA) configuration. Approximately 200 mg of powder were first shaped by uniaxial pressing (500 MPa) in a tungsten carbide die, resulting in a 5 mm diameter cylindrical pellet of about 1 mm in height. The linear shrinkage of the pellet was then followed as a function of temperature from RT to 1000°C with a heating rate of 1°C.min^{-1}. Thermal dilatation of alumina sample holder was measured under the same conditions and was subtracted from the resulting signal.

2.4. X-EDS

FEI Quanta 200 electron microscope equipped with X-EDS analyzer (BRUKER XFlash® 5010 SDD) was used for quantitative chemical analyses with an acceleration voltage of 15 kV and a chamber pressure below 2×10^{-4} Pa. The powdered samples were first embedded in an epoxy resin, polished to

mirror grade and then metalized. For each sample, 30 spots were analyzed and average values led to deduce the chemical composition of the samples.

2.5. Chemical compositions analyses with ICP-AES

In order to determine the composition of the synthesized rhabdophane samples, about 20 mg of the obtained powder was firstly dissolved completely in 2.5 mL aqua regia then diluted in 0.16 M HNO_3 solution. These solutions were analyzed through ICP-AES (Spectro Arcos EOP) after the application of SPEX standard solutions to calibrate the elementary concentrations of Ca, Th, Nd and P. The recommended emission wavelengths were taken into account in the calculation of elementary concentration leading to the evaluation of the atomic ratios.

3. Results

3.1. Synthesis of $Nd_{1-2x}Th_xCa_xPO_4 \cdot n\ H_2O$

According to the preparation method reported recently [32], thorium-bearing rhabdophane samples $Nd_{1-2x}Th_xCa_xPO_4 \cdot n\ H_2O$ with x = 0 to 0.15 were obtained by precipitation at 110°C during 4 days. PXRD analysis was performed to examine the crystal structure and showed that the powders were single phase rhabdophane (Figure 2). The chemical composition of the powders was then determined by ICP-AES after total dissolution of the samples in aqua regia (Table 1).

Table 1. Chemical composition of $Nd_{1-2x}Th_xCa_xPO_4 \cdot n\ H_2O$ rhabdophane-type compounds obtained by ICP-AES analysis after complete dissolution of the powdered samples

x (target value)	Nd (1-2x)	Th (x)	Ca (x)	P/(Nd+Ca+Th)
0.00	1.00 ± 0.01	---	---	1.04 ± 0.01
0.05	0.90 ± 0.01	0.05 ± 0.01	0.05 ± 0.01	1.0 ± 0.1
0.10	0.80 ± 0.03	0.11 ± 0.01	0.10 ± 0.01	1.0 ± 0.1
0.15	0.71 ± 0.03	0.17 ± 0.02	0.11 ± 0.02	1.1 ± 0.2

From these data, the prepared powders exhibited the expected stoichiometry for x = 0.05 and 0.1. However, the precipitation of thorium and calcium appeared to be slightly different from the expected values for x = 0.15. This problem was already described during the synthesis of $Pr_{1-2x}Th_xCa_xPO_4 \cdot nH_2O$ solid solutions, the precipitation becoming non-stoichiometric for $x \geq 0.20$ [32]. Consequently, the coupled substitution might exhibit a limit under these synthesis conditions. For Nd-based rhabdophane, the maximum Ca, Th incorporation might be between x = 0.10 and 0.15. Nevertheless, for x = 0.15, the charge balance seemed to be respected. Indeed, the total positive charge, i.e. 3 (Nd^{3+}) + 4 (Th^{4+}) + 2 (Ca^{2+}) equals 3.03 ± 0.21 while the total negative charge, i.e. 3 (PO_4^{3-}), reaches 3.21 ± 0.51. Both

values are thus not significantly different considering the associated uncertainties. One explanation of the slight difference between Th and Ca contents could result from the formation of the presence of vacancies in the structure. Additionally, it is worth noting that during the synthesis of $Pr_{1-2x}Th_xCa_xPO_4 \cdot n\ H_2O$ samples, XRD analysis revealed the formation of crystallized $Th_2(PO_4)_2(HPO_4) \cdot H_2O$ (TPHPH) [37] as a secondary phase for $x \geq 0.20$. Such an additional thorium-enriched phase was not detected by PXRD in this work which also argue in favor of a non-stoichiometric substitution.[37]

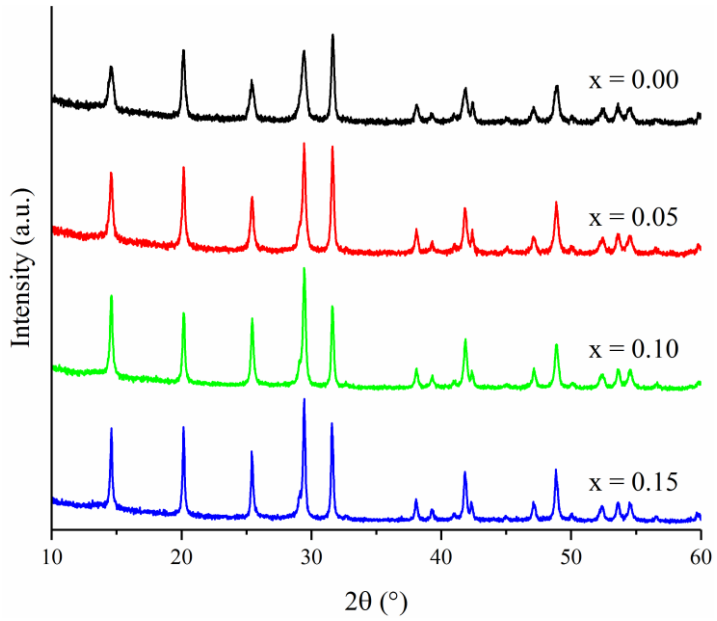

Figure 2. PXRD patterns obtained for $Nd_{1-2x}Th_xCa_xPO_4 \cdot nH_2O$ samples (with $0 \leq x \leq 0.15$)

3.2. Thermal conversion of $Nd_{1-2x}Th_xCa_xPO_4 \cdot n\ H_2O$ into $Nd_{1-2x}Th_xCa_xPO_4$

In order to achieve the conversion of rhabdophane into monazite, the synthesized precursors were first directly heated at 1100°C for 6 hours in air. According to the PXRD patterns collected on the resulting powders (Figure 3), the samples obtained from x = 0 to x = 0.10 were single phase monazite-cheralite solid solutions. Conversely, the presence of the XRD lines of α-ThP_2O_7 as secondary phase was evidenced for x = 0.15.[38]

In a previous work, Podor [39] prepared the monazite under hydrothermal conditions (780°C, 200 MPa) and reported that the direct substitution of thorium in the structure of $LaPO_4$ ($4\ La^{3+} \leftrightarrow 3\ Th^{4+} + \square$) was limited to only 7.45 ± 1.12 wt.% of ThO_2 (i.e. to 6.40 ± 0.99 mol.% of thorium). Above this value, thorium diphosphate (α-ThP_2O_7) always appeared as a secondary phase.[39] Therefore, for x = 0.15, the initial rhabdophane type structure, with a certain amount of vacancies and excess of Th, is no longer stable during its conversion into monazite-cheralite, leading to segregation of Th and thus to the formation of α-ThP_2O_7.

Since the monazite-cheralite solid solutions exhibited very high chemical durability, which resulted in only partial dissolution in fresh aqua regia under the application of the protocol developed for rhabdophane analysis (~ 0.020 mg sample in 2.5 mL aqua regia), the evaluation of their chemical composition was undertaken by X-EDS (Table 2). It is worth noting that the results obtained for monazite-cheralite solid solutions were not significantly different compared to that obtained for the starting rhabdophane samples, indicating the absence of phosphate elimination through decomposition during the heating treatment at high temperature.

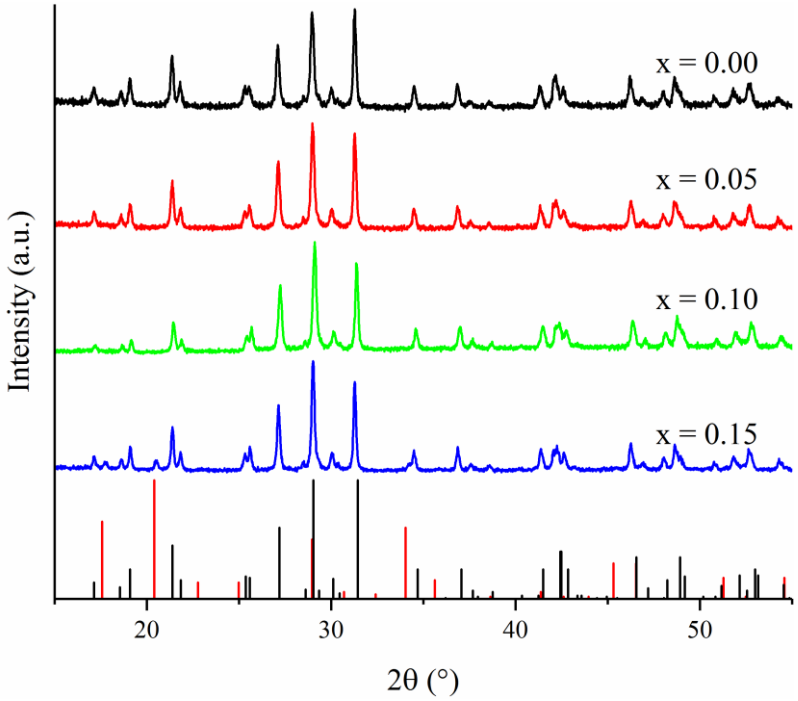

Figure 3. PXRD patterns obtained after conversion of $Nd_{1-2x}Th_xCa_xPO_4 \cdot n\ H_2O$ rhabdophanes at 1100°C for 6 hours (air atmosphere). PXRD patterns reported for monazite $NdPO_4$ (black vertical bars) [40] and for α-ThP_2O_7 (red vertical bars) [41].

Table 2. Results of X-EDS analysis obtained on $Nd_{1-2x}Th_xCa_xPO_4$ monazite-cheralite solid solution samples prepared after thermal conversion of rhabdophanes

x (target value)	Nd	Th	Ca	P/(Nd+Ca+Th)
0.05	0.86 ± 0.02	0.06 ± 0.01	0.07 ± 0.01	0.92 ± 0.05
0.10	0.76 ± 0.01	0.12 ± 0.01	0.11 ± 0.01	1.05 ± 0.03
0.15	0.67 ± 0.02	0.19 ± 0.02	0.14 ± 0.01	1.01 ± 0.05

3.3. Structural evolution followed by *in situ* HT-PXRD.

In order to get a better understanding of dehydration and conversion processes of $Nd_{1-2x}Th_xCa_xPO_4 \cdot n\ H_2O$ (x = 0.0 – 0.10), *in situ* HT-PXRD experiments were performed. The collected powder patterns recorded for $Nd_{0.8}Th_{0.1}Ca_{0.1}PO_4 \cdot n\ H_2O$ are viewed in Figure 4. This experiment underlined two phase

transitions: the first one took place at 200 °C while the second began at 700 °C and ended at 850 °C. The transition leading to the formation of the hemihydrate form reported previously by Mesbah *et al*.[35] was not detected on the basis of the quality of the data collected using a laboratory diffractometer. Therefore, in these experiments, the first transition observed led to the formation of anhydrous rhabdophane while the second one was assigned to the irreversible conversion into monazite-cheralite solid solution.

The *in situ* HT-PXRD patterns were then refined using the Rietveld method by considering the appropriate crystal structure depending on the temperature of the data collection, i.e.:

- i) at 30°C, the hydrated form $Nd_{1-2x}Th_xCa_xPO_4 \cdot 0.667\ H_2O$ (monoclinic C2, Z = 24);
- ii) between 100 and 200°C, the hemihydrate form $Nd_{1-2x}Th_xCa_xPO_4 \cdot 0.5\ H_2O$ (monoclinic C2 space group, Z = 12);
- iii) above 200°C, the trigonal form associated to anhydrous rhabdophane $Nd_{1-2x}Th_xCa_xPO_4$ ($P3_121$ space group, Z = 3).
- iv) above 700°C, the monoclinic form associated to the irreversible formation of monazite $Nd_{1-2x}Th_xCa_xPO_4$ ($P2_1/n$ space group, Z = 4).

Therefore, the unit cell volumes were systematically normalized to three formula units for each phase, underlining the variation of unit cell volume of $Nd_{1-2x}Th_xCa_xPO_4 \cdot n\ H_2O$ by direct comparison (Figure 5).

All the studied samples showed similar behavior. The structure change corresponding to the dehydration led to a volume swelling of about 1 % around 200°C. After a slight swelling due to the increase of temperature, the irreversible phase transition from anhydrous rhabdophane to monazite-cheralite solid solution occurred between 650°C and 850°C which agrees well with the transition temperature reported by Jonasson and Vance for $NdPO_4 \cdot 0.667\ H_2O$ (i.e. 680-790°C) [33]. Finally, the shrinkage of the unit cell volume reached 18.5%, confirming that the monazite-cheralite solid solutions have a far more compact structure than their rhabdophane counterparts.

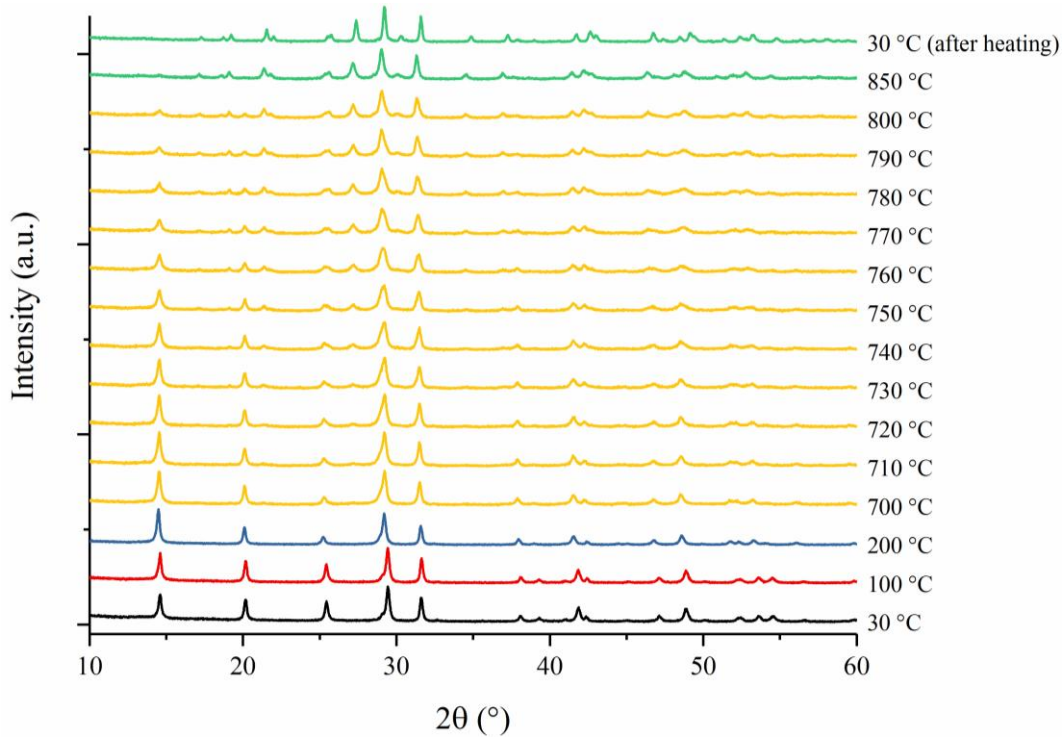

Figure 4. *In situ* HT-PXRD patterns of $Nd_{0.8}Th_{0.1}Ca_{0.1}PO_4 \cdot nH_2O$: initial rhabdophane (black line), hemihydrate rhabdophane (red line), anhydrous rhabdophane (blue line), mixture of rhabdophane and monazite-cheralite (yellow line) and single phase monazite-cheralite (green line).

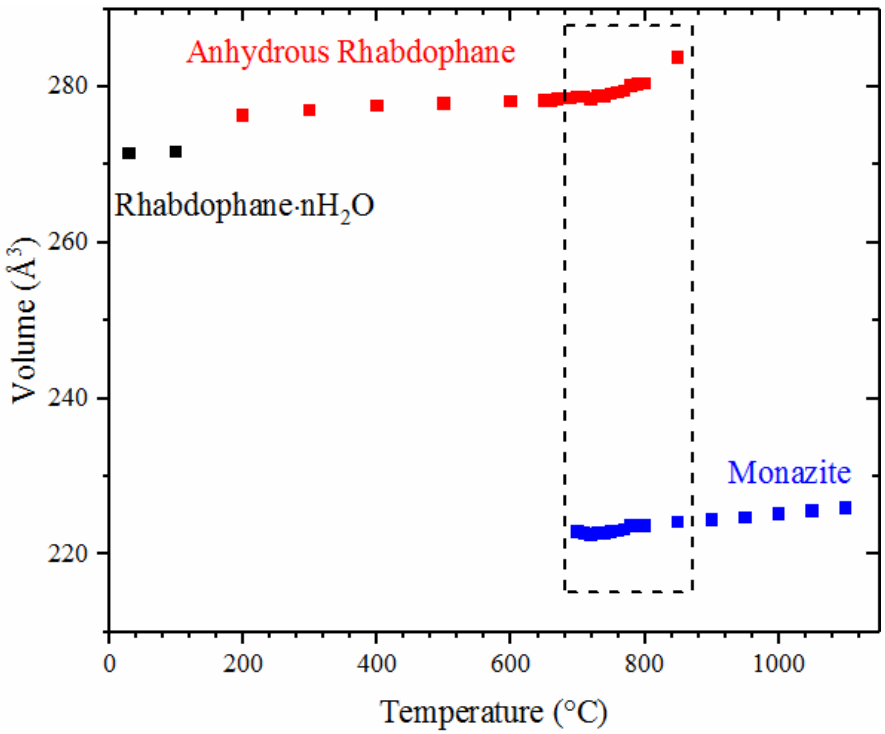

Figure 5. Variation of refined unit cell volume of $Nd_{0.8}Th_{0.1}Ca_{0.1}PO_4 \cdot nH_2O$ versus heating temperature, the volume of each phase was normalized to three formula units per cell for better understanding.

3.4. Thermo-Gravimetric Analysis

Even though *in situ* HT-PXRD experiment argued for a direct dehydration process is completed around 200 °C, it might go through several steps as in the case of lanthanide end-members [35]. Also, the amount of water molecules per unit formula has not been determined yet. TGA experiments were then performed to accurately follow the dehydration process of $Nd_{1-2x}Th_xCa_xPO_4 \cdot nH_2O$ ($0 \leq x \leq 0.10$) (Figure 6).

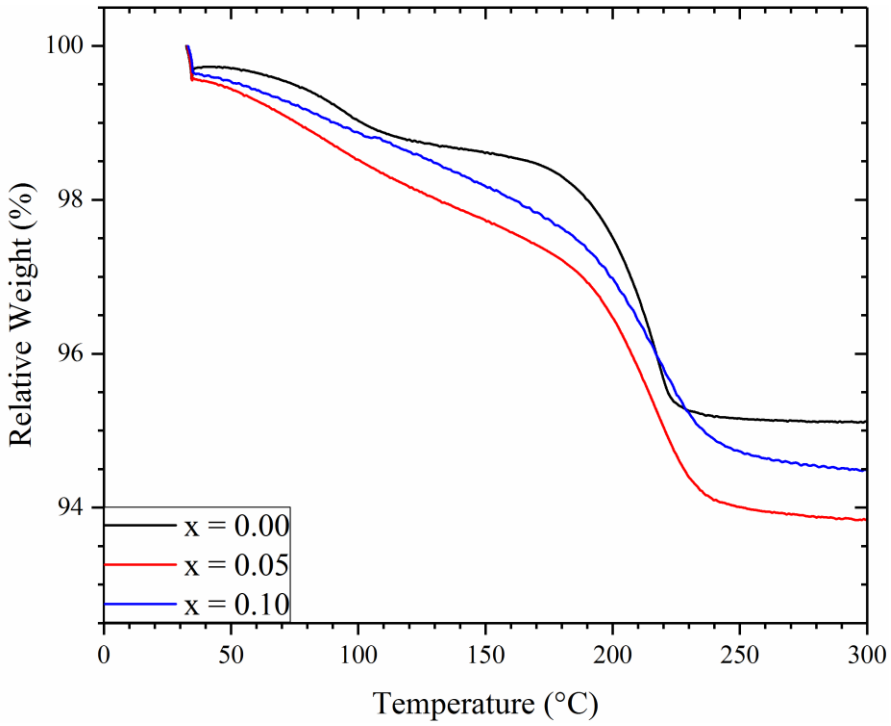

Figure 6. TGA curves obtained for $Nd_{1-2x}Th_xCa_xPO_4 \cdot nH_2O$ samples.

All the prepared samples exhibited similar dehydration process according to the TGA curves. Their water contents ranged from 0.68 ± 0.01 to 0.88 ± 0.01, which agrees with that proposed by Mesbah et al. (i.e. 0.667 H_2O per formula unit) [35, 42]. The DTG curves (Figure S1) showed that dehydration of $Nd_{1-2x}Th_xCa_xPO_4 \cdot n\ H_2O$ went through two successive steps leading to anhydrous rhabdophane structure type. In all cases, whatever the initial amount of water, the first dehydration led to the stable hemihydrate form, i.e. $Nd_{1-2x}Th_xCa_xPO_4 \cdot 0.5\ H_2O$, then to the anhydrous rhabdophane, i.e. $Nd_{1-2x}Th_xCa_xPO_4$. While the temperature associated to the first dehydration was difficult to determine, that corresponding to the full dehydration was extracted from the derivative of the relative weight. The obtained results are in agreement with those reported for the lanthanide rhabdophane end-members ($LnPO_4 \cdot 0.667H_2O$, with Ln = La to Dy) [35].

Table 3. Results of TGA obtained on $Nd_{1-2x}Th_xCa_xPO_4 \cdot n\ H_2O$ solid solutions

x	$T_{min\ derivative}$ (°C)	H_2O per unit formula (2^{nd} step)	H_2O per unit formula (total amount)
0.00	210 ± 3	0.46 ± 0.01	0.68 ± 0.01
0.05	213 ± 3	0.47 ± 0.01	0.88 ± 0.01
0.10	214 ± 3	0.46 ± 0.01	0.79 ±0.01

The incorporation of thorium and calcium within the structure has few impact on the temperature associated to the dehydration of the rhabdophane. Even though, the temperature of transition might increase very slightly with the incorporation rate of thorium and calcium in the structure as reported in Table 3.

3.5 Dilatometric study

The relative linear shrinkage of $Nd_{1-2x}Th_xCa_xPO_4 \cdot n\ H_2O$ was analyzed by dilatometric measurements (Figure 7) and revealed a three-step variation. The first dehydration step leading to the stabilization of the hemihydrate form was not observed. However, a slight swelling of about 1% took place around 200°C and was assigned to the complete dehydration of the rhabdophane compounds. Then a transition was observed from 600°C to 850°C and corresponds to the irreversible transformation from rhabdophane-type structure into monazite-cheralite which appears in good agreement with the results obtained from *in situ* HT-PXRD. The final step occurred at higher temperatures (i.e. for T > 850°C) and was correlated to the sintering of the samples.

The temperature of the phase transition, deduced from the maximum shrinkage rate, was found to increase with the Ca-Th coupled substitution rate from 693 ± 1°C (x = 0) to 762 ± 1°C (x = 0.1). It agreed well with the temperatures reported by Jonasson and Vance (500 – 900°C) and by Kijkowska (717 – 910°C) regarding to the formation of monazite endmembers[33, 43]. Moreover, both studies showed an increase of the transformation temperature with the atomic number. Reviewing the reported data and the results of this work, it might have an interest to investigate the variation of this temperature versus ionic radius. Indeed, as shown in Figure 8, such temperature of transformation was found to increase with the shrinkage of ionic radius.[44]

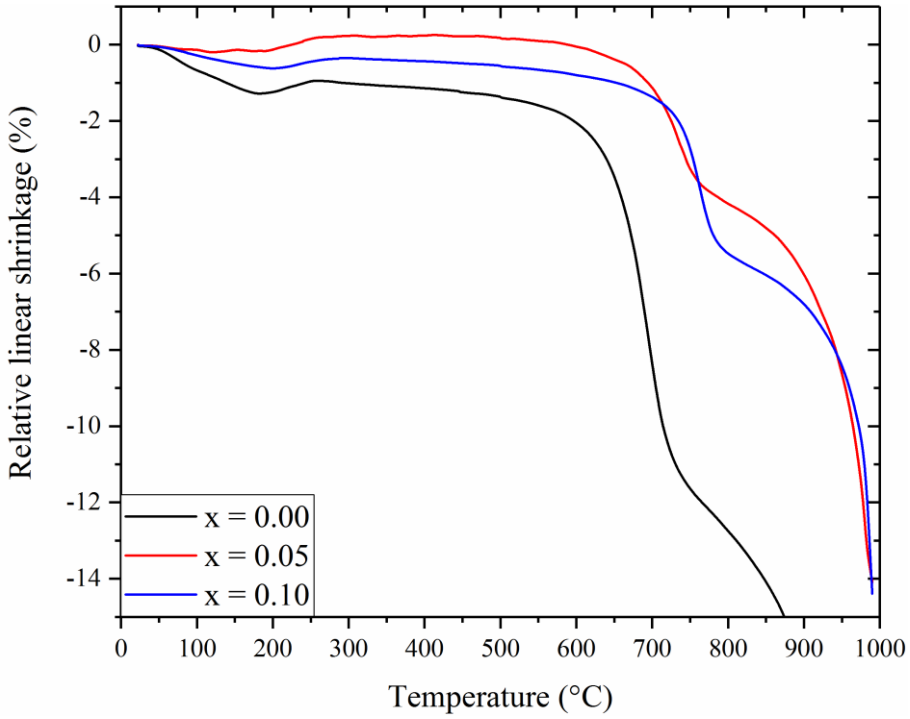

Figure 7. Dilatometric curves obtained during the sintering of $Nd_{1-2x}Th_xCa_xPO_4 \cdot n\ H_2O$ samples.

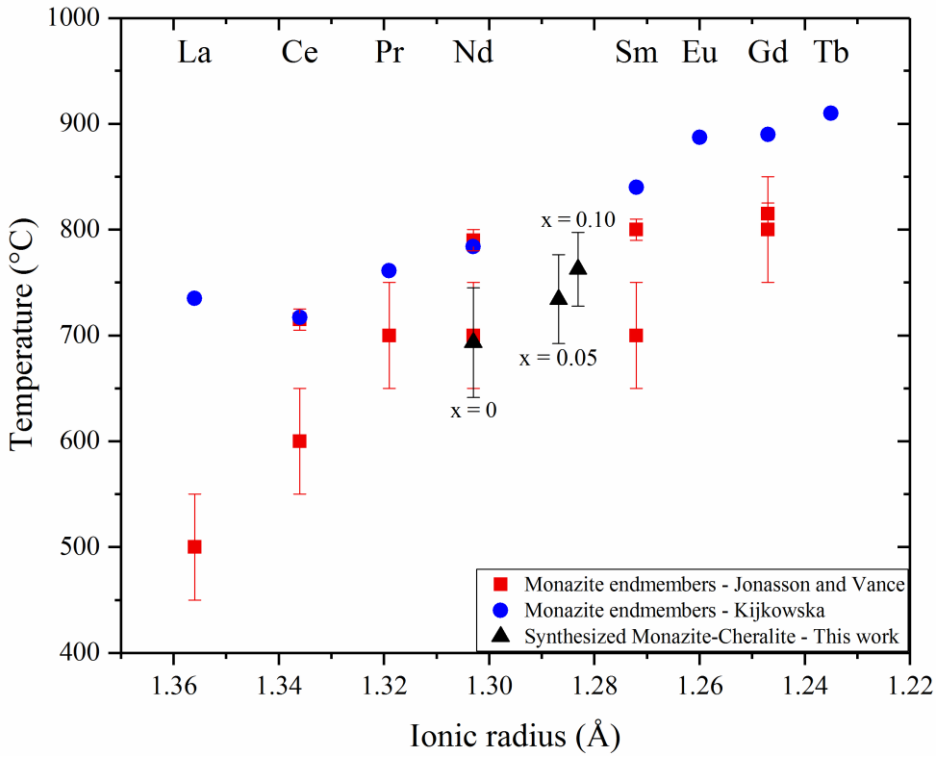

Figure 8. Variation of the the temperature ofconversion from rhabdophane to monazite-cheralite depending on the ionic radius.

3.5. Influence of coupled substitution on crystal structures

According to the TGA results, the first three temperature set points of the *in situ* HT-PXRD study, i.e. 30°C, 100°C and 300°C, were corresponding to three distinct phases, i.e. $Nd_{1-2x}Th_xCa_xPO_4 \cdot n\ H_2O$ (0.68 ± 0.01 to 0.88 ± 0.01), $Nd_{1-2x}Th_xCa_xPO_4 \cdot 0.5\ H_2O$ and $Nd_{1-2x}Th_xCa_xPO_4$, respectively. Based on such structural models, these collected PXRD patterns were refined by the Rietveld method. The variation of the unit cell volume of the $Nd_{1-2x}Th_xCa_xPO_4 \cdot nH_2O$ compounds are reported in Figure 9.

At 30°C, the rhabdophane crystallizes in the monoclinic system in C2 space group in the $LnPO_4.0.667\ H_2O$ structure type. The refined volume of the unit cell was found to increase when the thorium and calcium contents increase within the structure. If we consider the ionic radius of Nd^{3+}, Th^{4+} and Ca^{2+} reported in the Shannon tables (Table 4), the refined volume of the rhabdophane structure should decrease when smaller atoms are inserted. Such behavior could be explained by the preference of thorium and calcium to be coordinated by the water molecules leading to a 9-fold coordination. In this case, the volume of the unit cell should increase because the average r Ca-Th (CN =9) value is larger than the ionic radius of Nd (CN = 8), on the one hand, and because of the impact of larger amounts of water molecules within the channels, on the other hand. This assumption is justified also by the water content measured by TGA. Moreover, theoretically, if we consider that all the cationic sites are coordinated by water molecules, the structure should have 1.5 water molecule per formula unit.

Table 4. Selected Crystal Radius reported for Ca^{2+}, $Nd^{3+}$and Th^{4+}in the eight and nine fold coordination numbers [44]

Coordination	r_{Ca}^{2+} Å	r_{Th}^{4+} Å	$r_{Ca\text{-}Th}$ Å	r_{Nd}^{3+} Å	$\frac{\Delta(r_{Nd(VIII)} - r_{Ca\text{-}Th(IX)})}{r_{Nd(VIII)}}$
VIII	1.26	1.19	1.225	1.249	−2.1%
IX	1.32	1.23	1.275	1.303	

Despite the difficulties to determine the exact temperature of the first structural transition leading to the hemihydrate form, we can suggest that its stabilization occurs below 100°C. Therefore, the difference of the relative weight between 100°C and over 250 °C is corresponding to about 0.5 H_2O (TGA results, Table 3). According to the data viewed in Figure 9, after the first dehydration step, the unit cell volume seemed to decrease in agreement with the ionic radius of Th^{4+}, Ca^{2+} and Nd^{3+} reported in literature [44]. Regarding the structural features of the hemihydrate form (Figure 1), we could assume that there is no ordering of thorium and calcium on a specific site (i.e. specific coordination number), and thus the distribution of water molecules respects the crystal structure properties published previously by Mesbah et al. [35]. Moreover, the same observation was made for the structure refined at

300°C when considering the anhydrous form of the rhabdophane structure. It is worth noting that the unit cell volume variations at 100°C and 300°C were consistent with that expected. Therefore, there is more reason to believe that the increase of the unit cell volume of $Nd_{1-2x}Th_xCa_xPO_4 \cdot n\ H_2O$ compounds collected at 30°C could be associated to the increase of water amounts within the channels.

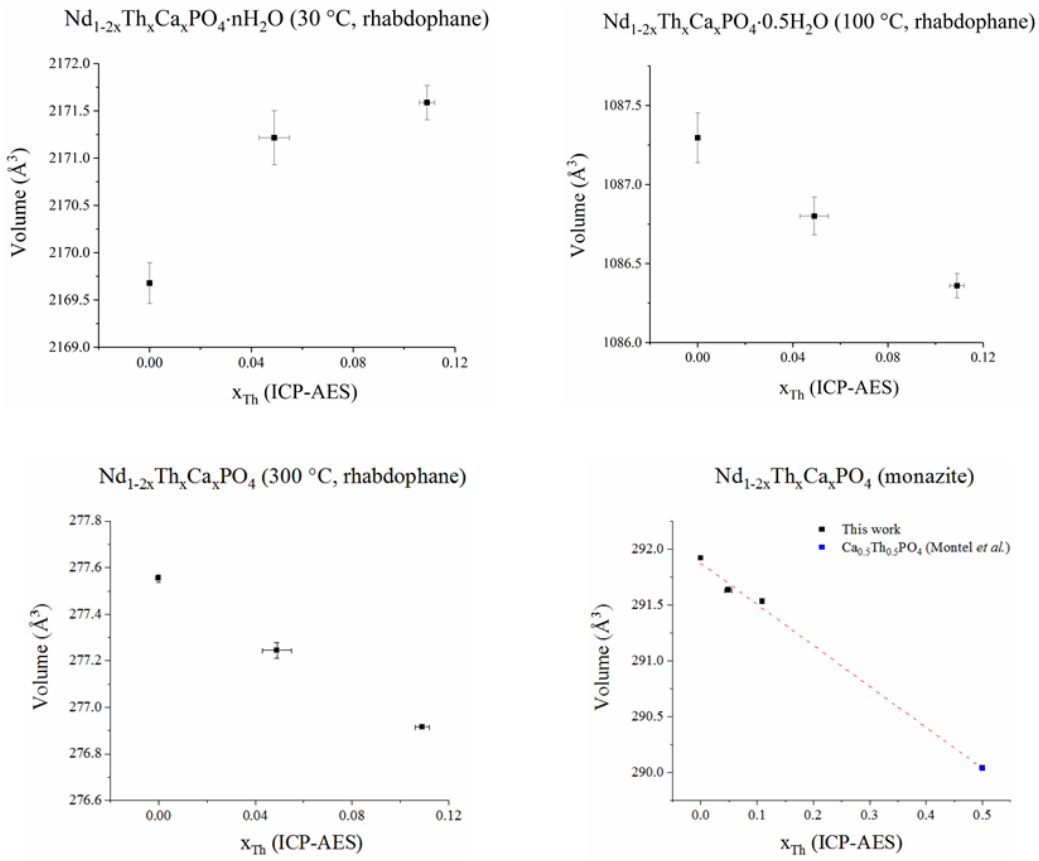

Figure 9. Refined unit cell volume obtained for $Nd_{1-2x}Th_xCa_xPO_4 \cdot n\ H_2O$ samples prepared at 30°C, 100°C, 300°C and those corresponding to the monazite-cheralite samples collected at 30°C after thermal treatment at 1100°C.

At higher temperatures, anhydrous rhabdophane underwent an irreversible transition into the monazite-cheralite structure type crystallizing in the monoclinic system ($P2_1/n$ space group). Hereby, XRD patterns were recorded back at RT to avoid any bias due to high-temperature collection. The unit cell volume of $Ca_{0.5}Th_{0.5}PO_4$ end-member [25] was introduced to compare with those of the $Nd_{1-2x}Th_xCa_xPO_4$ series. The unit cell volume decreased linearly with the incorporation rate following the Vegard's law. Such a variation thus suggests the formation of an ideal $Nd_{1-2x}Th_xCa_xPO_4$ solid solution (Figure 9). [32]

4. Conclusions

In this study, rhabdophane-type precursors with general formula $Nd_{1-2x}Th_xCa_xPO_4 \cdot n\ H_2O$ (x = 0 to 0.15) were prepared by hydrothermal synthesis. Single phase monazite-cheralite $Nd_{1-2x}Th_xCa_xPO_4$ solid solutions were obtained by direct heating of such precursors from x = 0 to x = 0.1. For x > 0.1, the composition of the rhabdophane precursor appeared to be non-stoichiometric and α-ThP_2O_7 was found as a secondary phase in the final product. The combination of TGA analyses, HT-PXRD and dilatometry experiments allowed the description of the thermal conversion of rhabdophane-type precursor to the final monazite-cheralite wasteform. The temperatures associated to the dehydration and to the rhabdophane to monazite conversion were determined. The Ca-Th coupled substitution rate seemed to affect these transformation temperatures as the change of ion radii would influence the structure stability. In the case of the as-synthesized powders, the refined unit cell volume was found to increase when smaller atoms are incorporated within the structure. This unexpected trend is impacted by the insertion of extra water molecules in a slightly variable amounts within the channels. Accurate determination of the temperature associated to the stabilization of the hemihydrate form was not possible. However, above 100°C, we assume all the samples prepared to be under the form $Nd_{1-2x}Th_xCa_xPO_4 \cdot 0.5\ H_2O$ (x = 0 to 0.10). Under these circumstances, the unit cell volume decreases linearly in agreement with the average size of Ca-Th incorporated in the structure. At higher temperature ($\geq$ 210°C), the anhydrous form is observed and above 650°C the monazite-cheralite structure is irreversibly stabilized. In agreement with the previous studies, the temperature of transition rhabdophane-monazite was found to increase with the average ionic size of cations. Based on this thermal behavior and aiming at the use of such ceramics for the long-term conditioning of radioactive waste, further experiments will be focused on the sintering properties as well as on the chemical durability of the prepared materials.

Acknowledgements

The authors would like to express their gratitude to Bruno Corso (ICSM) for the PXRD measurement; Renaud Podor and Joseph Lautru (ICSM) for X-EDS analyses. PhD salary of Danwen Qin was funded by the China Scholarship Council (CSC).

AUTHORS INFORMATION

*E-mail: adel.mesbah@cea.fr (A. MESBAH)

Nicolas.clavier@icsm.fr (N. Clavier)

Notes

The authors declare no competing financial interest.

References:

1. Ewing, R. C. Nuclear waste forms for actinides. *Proceedings of the National Academy of Sciences of the United States of America* **1999,** 96 (7), 3432-3439.
2. Lutze, W.; Ewing, R. *Radioactive waste forms for the future*. North Holland, 1988.
3. Loiseau, P.; Caurant, D.; Baffier, N.; Mazerolles, L.; Fillet, C. Glass–ceramic nuclear waste forms obtained from SiO_2–Al_2O_3–CaO–ZrO_2–TiO_2 glasses containing lanthanides (Ce, Nd, Eu, Gd, Yb) and actinides (Th): study of internal crystallization. *J. Nucl. Mater.* **2004,** 335 (1), 14-32.
4. Deschanels, X. *Evaluation of the technical feasibility of new conditioning matrices for long-lived radionuclides*; INIS-FR--5692; France, 2004; p 112.
5. Bros, R.; Carpena, J.; Sere, V.; Beltritti, A. Occurrence of Pu and fissiogenic REE in hydrothermal apatites from the fossil nuclear reactor 16 at Oklo (Gabon). *Radiochimica Acta* **1996,** 74, 277-282.
6. Terra, O.; Audubert, F.; Dacheux, N.; Guy, C.; Podor, R. Synthesis and characterization of thorium-bearing britholites. *Journal of Nuclear Materials* **2006,** 354 (1), 49-65.
7. Terra, O.; Audubert, F.; Dacheux, N.; Guy, C.; Podor, R. Synthesis and characterization of uranium-bearing britholites. *Journal of Nuclear Materials* **2007,** 366 (1), 70-86.
8. Tabuteau, A.; Pages, M.; Livet, J.; Musikas, C. Monazite-like phase containing transuranium elements (neptunium and plutonium). *Journal of Materials Science Letters* **1988,** 7 (12), 1315-1317.
9. Meldrum, A.; Boatner, L. A.; Weber, W. J.; Ewing, R. C. Radiation damage in zircon and monazite. *Geochimica et Cosmochimica Acta* **1998,** 62 (14), 2509-2520.
10. Dacheux, N.; Clavier, N.; Podor, R. Monazite as a promising long-term radioactive waste matrix: Benefits of high-structural flexibility and chemical durability. *American Mineralogist* **2013,** 98 (5-6), 833-847.
11. Kitaev, D. B.; Volkov, Y. F.; Orlova, A. I. Orthophosphates of Tetravalent Ce, Th, U, Np, and Pu with the Monazite Structure. *Radiochemistry* **2004,** 46 (3), 211-217.
12. Terra, O.; Dacheux, N.; Audubert, F.; Podor, R. Immobilization of tetravalent actinides in phosphate ceramics. *Journal of Nuclear Materials* **2006,** 352 (1), 224-232.
13. Benard, P.; Brandel, V.; Dacheux, N.; Jaulmes, S.; Launay, S.; Lindecker, C.; Genet, M.; Louer, D.; Quarton, M. $Th_4(PO_4)_4P_2O_7$, a new thorium phosphate: Synthesis, characterization, and structure determination. *Chemistry of Materials* **1996,** 8 (1), 181-188.
14. Bregiroux, D.; Terra, O.; Audubert, F.; Dacheux, N.; Serin, V.; Podor, R.; Bernache-Assollant, D. Solid-state synthesis of monazite-type compounds containing tetravalent elements. *Inorganic Chemistry* **2007,** 46 (24), 10372-10382.
15. Davis, D. D.; Vance, E. R.; McCarthy, G. J. *Crystal chemistry and phase relations in the synthetic minerals of ceramic waste forms. II. Studies of uranium-containing monazites*. Plenum Press: United States, 1981.
16. Terra, O.; Clavier, N.; Dacheux, N.; Podor, R. Preparation and characterization of lanthanum-gadolinium monazites as ceramics for radioactive waste storage. *New J. Chem.* **2003,** 27 (6), 957-967.
17. Lumpkin, G. R.; Geisler-Wierwille, T. In *Comprehensive Nuclear Materials*; Elsevier: Oxford, 2012; pp 563-600.
18. Boatner, L. A.; Sales, B. C. *Radioactive Waste Forms for the Future*. North-Holland Physics Publishing: Amsterdam, 1988; p 495.
19. Deschanels, X.; Seydoux-Guillaume, A. M.; Magnin, V.; Mesbah, A.; Tribet, M.; Moloney, M. P.; Serruys, Y.; Peuget, S. Swelling induced by alpha decay in monazite and zirconolite ceramics: A XRD and TEM comparative study. *Journal of Nuclear Materials* **2014,** 448 (1–3), 184-194.
20. Seydoux-Guillaume, A.-M.; Deschanels, X.; Baumier, C.; Neumeier, S.; Weber William, J.; Peuget, S., Why natural monazite never becomes amorphous: Experimental evidence for alpha self-healing. In *American Mineralogist*, 2018; Vol. 103, p 824.
21. Burakov, B. E.; Yagovkina, M. A.; Garbuzov, V. M.; Kitsay, A. A.; Zirlin, V. A. Self-Irradiation of Monazite Ceramics: Contrasting Behavior of $PuPO_4$ and $(La,Pu)PO_4$ Doped with Pu-238. *MRS Proceedings* **2004,** 824,
22. Bregiroux, D.; Belin, R.; Valenza, P.; Audubert, F.; Bernache-Assollant, D. Plutonium and americium monazite materials: Solid state synthesis and X-ray diffraction study. *J. Nucl. Mater.* **2007,** 366 (1), 52-57.

23. Hikichi, Y.; Hukuo, K.-i.; Shiokawa, J. Solid solutions in the systems monazite($CePO_4$)-huttonite($ThSiO_4$), and monazite-$Ca_{0.5}Th_{0.5}PO_4$. *Nippon Kagaku Kaishi* **1978,** 1978 (12), 1635-1640.
24. Hughes, J.; Foord, E.; Hubbard, M.; Ni, Y. The Crystal-Structure of Cheralite-(Ce),(LREE, Ca, Th, U)(P, Si)O_4, a Monazite-Group Mineral. *Neues Jahrbuch fur Mineralogie-Monatshefte* **1995,** (8), 344-350.
25. Montel, J. M.; Devidal, J. L.; Avignant, D. X-ray diffraction study of brabantite-monazite solid solutions. *Chemical Geology* **2002,** 191 (1-3), 89-104.
26. Brandel, V.; Dacheux, N. Chemistry of tetravalent actinide phosphates—Part II. *Journal of Solid State Chemistry* **2004,** 177 (12), 4755-4767.
27. Raison, P. E.; Jardin, R.; Bouëxière, D.; Konings, R. J. M.; Geisler, T.; Pavel, C. C.; Rebizant, J.; Popa, K. Structural investigation of the synthetic $CaAn(PO_4)_2$ (An = Th and Np) cheralite-like phosphates. *Physics and Chemistry of Minerals* **2008,** 35 (10), 603-609.
28. Clavier, N.; Podor, R.; Dacheux, N. Crystal chemistry of the monazite structure. *Journal of the European Ceramic Society* **2011,** 31 (6), 941-976.
29. Popa, K.; Cologna, M.; Martel, L.; Staicu, D.; Cambriani, A.; Ernstberger, M.; Raison, P. E.; Somers, J. $CaTh(PO_4)_2$ cheralite as a candidate ceramic nuclear waste form: Spark plasma sintering and physicochemical characterisation. *Journal of the European Ceramic Society* **2016,** 36 (16), 4115-4121.
30. Podor, R.; Cuney, M. Experimental study of Th-bearing $LaPO_4$ (780 °C, 200 MPa): Implications for monazite and actinide orthophosphate stability. *American Mineralogist* **1997,** 82 (7-8), 765-771.
31. Du Fou de Kerdaniel, E.; Clavier, N.; Dacheux, N.; Terra, O.; Podor, R. Actinide solubility-controlling phases during the dissolution of phosphate ceramics. *Journal of Nuclear Materials* **2007,** 362 (2-3), 451-458.
32. Qin, D.; Mesbah, A.; Gausse, C.; Szenknect, S.; Dacheux, N.; Clavier, N. Incorporation of thorium in the rhabdophane structure: Synthesis and characterization of $Pr_{1-2x}Ca_xTh_xPO_4{\cdot}nH_2O$ solid solutions. *J. Nucl. Mater.* **2017,** 492 (Supplement C), 88-96.
33. Jonasson, R. G.; Vance, E. R. DTA STUDY OF THE RHABDOPHANE TO MONAZITE TRANSFORMATION IN RARE-EARTH (LA-DY) PHOSPHATES. *Thermochimica Acta* **1986,** 108, 65-72.
34. Kijkowska, R. Thermal decomposition of lanthanide orthophosphates synthesized through crystallisation from phosphoric acid solution. *Thermochimica Acta* **2003,** 404 (1-2), 81-88.
35. Mesbah, A.; Clavier, N.; Elkaim, E.; Szenknect, S.; Dacheux, N. In pursuit of the rhabdophane crystal structure: from the hydrated monoclinic $LnPO_4.0.667H_2O$ to the hexagonal LnPO4 (Ln = Nd, Sm, Gd, Eu and Dy). *Journal of Solid State Chemistry* **2017,** 249, 221-227.
36. Frontera, C.; Rodriguez-Carvajal, J. FULLPROF as a new tool for flipping ratio analysis. *Physica B-Condensed Matter* **2003,** 335 (1-4), 219-222.
37. Brandel, V.; Dacheux, N.; Genet, M.; Podor, R. Hydrothermal synthesis and characterization of the thorium phosphate hydrogenphosphate, thorium hydroxide phosphate, and dithorium oxide phosphate. *Journal of Solid State Chemistry* **2001,** 159 (1), 139-148.
38. Clavier, N.; Wallez, G.; Dacheux, N.; Bregiroux, D.; Quarton, M.; Beaunier, P. Synthesis, Raman and Rietveld analysis of thorium diphosphate. *Journal of Solid State Chemistry* **2008,** 181 (12), 3352-3356.
39. Podor, R. Synthèse et caractérisation des monazites uranifères et thorifères. Université Henri Poincaré Nancy I, 1994.
40. Mooney, R. C. L. Crystal structures of a series of rare earth phosphates. *Journal of Chemical Physics* **1948,** 16 (10), 1003-1003.
41. Burdese, A.; Lucco, B.; Annali, M. *Ann. Chim. (Rome)* **1963,** 53, 333.
42. Mesbah, A.; Clavier, N.; Elkaim, E.; Gausse, C.; Ben Kacem, I.; Szenknect, S.; Dacheux, N. Monoclinic Form of the Rhabdophane Compounds: $REEPO_4{\cdot}0.667H_2O$. *Cryst. Growth Des.* **2014,** 14 (10), 5090-5098.
43. Kijkowska, R. Thermal decomposition of lanthanide orthophosphates synthesized through crystallisation from phosphoric acid solution. *Thermochim. Acta* **2003,** 404 (1), 81-88.
44. Shannon, R. D. Revised effective inonic-radii and systematic studies of interatomic distances in halides and chalcogenides. *Acta Crystallogr. Sect. A* **1976,** 32 (SEP1), 751-767.

FOR TABLE OF CONTENTS USE ONLY

Authors: Danwen Qin, Adel Mesbah, Nicolas Clavier, Stéphanie Szenknect, Nicolas Dacheux

Synopsis. $Nd_{1-2x}Th_xCa_xPO_4 \cdot n\ H_2O$ (x = 0 – 0.15) solid solutions were prepared under hydrothermal conditions (110°C, t = 4 days). The combined *in situ* high temperature PXRD, TGA and dilatometry investigations showed that the dehydration process follows the same trend than the $NdPO_4 \cdot 0.667\ H_2O$ end-member. The incorporation of Ca/Th was found to increase slightly the dehydration temperature (210±3°C to 214±3°C) as well as that corresponding to the irreversible conversion into monazite at higher temperature (693±1°C to 762±1°C).